

## Structural, electrical, and wettability properties of self-supporting PVDF/TiO<sub>2</sub>/GO composite films obtained by a solvent evaporation route

<http://dx.doi.org/10.1590/0370-44672023770014>

**Maria Luiza A. Almeida**<sup>1,5</sup>

<https://orcid.org/0009-0001-9365-3101>

**Millena A. Fernandes**<sup>1,6</sup>

<https://orcid.org/0000-0002-1614-3132>

**Hugo G. Palhares**<sup>1,7</sup>

<https://orcid.org/0000-0001-6813-2999>

**Lucas M.C. Silva**<sup>1,8</sup>

<https://orcid.org/0000-0003-1227-0377>

**Ludmila G. O. Xavier**<sup>2,9</sup>

<https://orcid.org/0000-0002-4070-0955>

**Tulio Matencio**<sup>2,10</sup>

<https://orcid.org/0000-0002-5660-8125>

**Liliane A. Silva**<sup>3,11</sup>

<https://orcid.org/0000-0003-3123-7695>

**Luiz O. Faria**<sup>3,12</sup>

<https://orcid.org/0000-0001-8159-4442>

**Vinicius G. de Castro**<sup>4,13</sup>

<https://orcid.org/0000-0002-1373-5909>

**Tarcizo C. de Souza**<sup>4,14</sup>

<https://orcid.org/0000-0001-6437-0009>

**Manuel Houmard**<sup>2,4,15</sup>

<https://orcid.org/0000-0002-1543-5416>

**Eduardo H.M. Nunes**<sup>1,4,16</sup>

<https://orcid.org/0000-0001-6653-5137>

<sup>1</sup>Universidade Federal de Minas Gerais - UFMG, Departamento de Engenharia Metalúrgica e de Materiais (DEMET), Belo Horizonte - Minas Gerais - Brasil.

<sup>2</sup>Universidade Federal de Minas Gerais - UFMG), Departamento de Química, Belo Horizonte - Minas Gerais - Brasil.

<sup>3</sup>Centro de Desenvolvimento da Tecnologia Nuclear, Belo Horizonte - Minas Gerais - Brasil.

<sup>4</sup>Centro de Tecnologia em Nanomateriais e Grafeno, Belo Horizonte - Minas Gerais - Brasil.

E-mails: <sup>5</sup>[marialuizaalmeida@hotmail.com](mailto:marialuizaalmeida@hotmail.com),

<sup>6</sup>[mellenafernandes18@gmail.com](mailto:mellenafernandes18@gmail.com),

<sup>7</sup>[hugogpalhares@gmail.com](mailto:hugogpalhares@gmail.com),

<sup>8</sup>[lucasmarton89@gmail.com](mailto:lucasmarton89@gmail.com), <sup>9</sup>[ludmilaqui@gmail.com](mailto:ludmilaqui@gmail.com),

<sup>10</sup>[tulmatencio@gmail.com](mailto:tulmatencio@gmail.com), <sup>11</sup>[lasfisica@gmail.com](mailto:lasfisica@gmail.com),

<sup>12</sup>[farialo@cdtn.br](mailto:farialo@cdtn.br), <sup>13</sup>[viniciusgomide12@gmail.com](mailto:viniciusgomide12@gmail.com),

<sup>14</sup>[tarcizocruz@gmail.com](mailto:tarcizocruz@gmail.com), <sup>15</sup>[mhoumard@ufmg.br](mailto:mhoumard@ufmg.br),

<sup>16</sup>[eduardo.nunes@demet.ufmg.br](mailto:eduardo.nunes@demet.ufmg.br)

### Abstract

Polyvinylidene fluoride (PVDF) is a versatile and low-cost polymer with high biocompatibility, mechanical strength, chemical resistance, thermal stability, and ferroelectricity. This material has been widely used in many applications, ranging from membranes to electronic devices. In this study, self-supporting, flexible, and lightweight PVDF films were prepared by an evaporation route using a low-toxicity solvent (dimethyl sulfoxide – DMSO). Graphene oxide (GO) and anatase titania (TiO<sub>2</sub>) were incorporated into the PVDF after preparing DMSO-based suspensions of these materials. The prepared materials were examined in terms of their structural, electrical, and wetting properties before and after exposure to near ultraviolet (UV-A) light. Substantial structural changes took place after incorporating GO and TiO<sub>2</sub> into PVDF. Such modifications were accompanied by dramatic changes in the wetting and electrical properties of the PVDF. UV-A light caused the formation of surface defects on PVDF and GO films. In addition, it promoted the photoreduction of GO into reduced graphene oxide (rGO). Composites containing TiO<sub>2</sub> showed high resistance to UV-A light, probably because titania particles absorb the incoming photons and shield the polymer matrix. This study provides new insights into the synthesis and characterization of PVDF/TiO<sub>2</sub>/GO composite films, which may be useful for many applications, including flexible electronics, solar cells, and biomedical devices.

**Keywords:** PVDF; graphene oxide; films; crystallization; irradiation; electrical properties.

## 1. Introduction

Polyvinylidene fluoride (PVDF) is a versatile polymer widely used in many applications (Athanasakou *et al.*, 2019; Thamizhlarasan *et al.*, 2022), including membranes (Hu *et al.*, 2022), catalysts (Altomare & Loos, 2023), and biomedical devices (Palwai *et al.*, 2022). This is due to its low cost, biocompatibility, high mechanical strength, good chemical resistance, high thermal stability, and ferroelectricity (Saxena & Shukla, 2021; Yin *et al.*, 2022). PVDF is a thermoplastic linear polymer and a semi-crystalline material, where amorphous and crystalline phases may coexist. Its main crystalline phases are: alpha ( $\alpha$ ), beta ( $\beta$ ), and gamma ( $\gamma$ ). The  $\alpha$ -phase is non-polar and has a TGTG (trans-gauche-trans-gauche) conformation, while the  $\beta$ -phase is highly-polar and has a TTTT (trans-trans-trans-trans) conformation. The  $\gamma$ -phase has a TTTG (trans-trans-trans-gauche) conformation (Piedrahita-Bello, 2020) and is commonly obtained from the rapid cooling of melt solutions (Wang *et al.*, 2018). Among these three phases, the  $\beta$ -phase has the highest dipole moment (about  $8 \times 10^{-30}$  C.m) (Correia & Ramos, 2005) and gives high piezoelectricity to PVDF. Such behavior is due to the arrangement of H and F atoms in the  $\beta$ -phase, where they are attached to the chain, such that the dipole moments associated with two C–H and two C–F bonds align up in the direction perpendicular to the carbon backbone (Kabir *et al.*, 2017). The combination of these electronic properties and flexibility makes this polymer a promising candidate for preparing self-powered electronic skins (e-skins)

## 2. Materials and methods

### 2.1. Processing - GO suspension

A solution of sulfuric acid (Synth, 98%, 360 mL) and potassium permanganate (Neon, 99%, 15 g) was initially prepared under stirring in an ice bath. Next, graphite powder (CBG Mining, 7.5 g) was added to this solution. The as-prepared suspension was kept in a microwave system (Milestone Star D)

### - Sol-gel synthesis of TiO<sub>2</sub> anatase

Titanium tetraisopropoxide (TTIP, Aldrich, 98%) was initially dissolved in absolute ethanol (EtOH, Aldrich,  $\geq$

for health monitoring (Mahanty *et al.*, 2020; Miki *et al.*, 2019).

Titania (TiO<sub>2</sub>) nanoparticles and graphene oxide (GO) nanosheets have been incorporated into PVDF, aiming to obtain materials for use as a separator in lithium-ion batteries (Khasbi, Youssefi and Semnani, 2020), antifouling membranes (Du *et al.*, 2019; Mohamat *et al.*, 2021), self-cleaning and ultraviolet (UV) light-resistant coatings (Liu, Zhanjian *et al.*, 2021), and photocatalytic materials (Abdelmaksoud *et al.*, 2021). TiO<sub>2</sub> is probably the most investigated semiconductor, having three main polymorphic phases, namely anatase, rutile, and brookite (Hanaor & Sorrell, 2011). Anatase is the most photoactive polymorph of titania (Bosc, Ayrat and Guizard, 2005), but rutile is also used as a photocatalyst (Marra *et al.*, 2022). Brookite is challenging to prepare and unstable at room temperature and pressure, which is why it has not been extensively studied (Liu, Lianjun *et al.*, 2012). The photocatalytic properties of titania are associated with the creation of electron-hole pairs during its exposition to UV light. In this step, electrons are promoted from the valence band to the conduction band, giving rise to holes in the former band. The high photoactivity of anatase is due to its small particle size and high specific surface area compared to rutile and brookite. Moreover, anatase has a low electron-hole recombination rate, which also contributes to its photoactivity (Zhang *et al.*, 2014). GO has also been combined with TiO<sub>2</sub> to increase the lifetime of these charge carriers. To achieve this, GO is reduced to rGO (reduced graphene oxide) because the latter has no

operating at 250 W and 70 °C for 10 min. The suspension was then dispersed in deionized water, and an aqueous solution of hydrogen peroxide (35%) was added to remove impurities. The suspension was filtered and the remaining solid (graphite oxide) was washed with water to pH 7. GO was obtained after the ultrasonic

98%). EtOH, hydrochloric acid (HCl, Aldrich, 37%), and deionized water were added to another flask. After

bandgap and is a good electrical conductor. Thus, electrons and holes can diffuse to rGO, making their recombination less likely to occur (Gonçalves; Palhares; *et al.*, 2019). Different approaches have been used to convert GO into rGO, including thermal annealing (Chua & Pumera, 2014), chemical reduction (Silva *et al.*, 2017), and microwave reduction (Jakha, Yap and Joshi, 2020). Photoreduction of GO with near-ultraviolet (UV-A) light has also recently been reported as a promising approach (Silva, L.M.C. *et al.*, 2021).

In this study, PVDF was initially mixed with dimethyl sulfoxide (DMSO), a low-toxicity solvent widely used in the food and pharmaceutical industries (McKim & Strub, 2008; Russo *et al.*, 2020). Many studies use hazardous solvents, such as N,N-dimethylformamide, N-methyl pyrrolidone, or N, N-dimethylacetamide (Karimi *et al.*, 2020), which makes these approaches unfeasible for many applications. A colloidal suspension of TiO<sub>2</sub> was obtained by a sol-gel route, while a suspension of GO nanosheets was prepared after the ultrasonic exfoliation of graphite powder. PVDF/TiO<sub>2</sub>/GO composites were obtained from these suspensions. After drying in air, the as-prepared films were examined according to their structural, electrical, and wettability properties. The influence of the UV-A light on these properties was also evaluated. A series of tests was employed here, including X-ray diffraction (XRD), Fourier transform infrared spectroscopy (FTIR), differential scanning calorimetry (DSC), scanning electron microscopy (SEM), atomic force microscopy (AFM), and electrochemical impedance spectroscopy (EIS).

exfoliation of the graphite oxide in water for 30 min. The suspension was centrifuged at 4000 rpm for 20 min and GO was collected as a supernatant (Castro *et al.*, 2017). GO was then dried and DMSO was added to disperse GO in this solvent. The concentration of GO in this suspension was about 4 g.L<sup>-1</sup>.

homogenization, these solutions were mixed under stirring and aged at room temperature for about two days. Deion-

ized water was added and the molar ratio of TTIP: EtOH: HCl: H<sub>2</sub>O was adjusted to 1: 35: 0.3: 90.3. The solution was transferred to a Teflon-lined stainless steel autoclave and kept at 130 °C

### - TiO<sub>2</sub>-GO dispersion

The previously prepared suspension of GO (4 g.L<sup>-1</sup>) was mixed with the colloidal suspension of TiO<sub>2</sub> under

### - PVDF/TiO<sub>2</sub>/GO films

PVDF pellets (Aldrich, Mw = 180,000 g.mol<sup>-1</sup>) were initially dissolved in DMSO (Aldrich, 99.9%) under sonication at 50 °C. Each 0.03 g of PVDF was dissolved in 1 mL of DMSO. The as-obtained solution was used to prepare PVDF/TiO<sub>2</sub>/GO composite films. PVDF, PVDF/TiO<sub>2</sub>, and PVDF/GO films were also obtained for reference purposes. PVDF/TiO<sub>2</sub> films were obtained by

for 6 h leading to the formation of anatase nanoparticles, as described elsewhere (Gonçalves & Souza; *et al.* 2019; Palhares, Nunes and Houmard, 2021). An exchange procedure was subsequently conducted to

stirring at room temperature for 1 h and under sonication for another 1 h. The concentration of GO in this suspension

mixing the PVDF/DMSO solution and TiO<sub>2</sub> suspension under sonication at 50 °C for 90 min. PVDF/GO films were prepared by mixing PVDF/DMSO and GO/DMSO solutions under sonication at 50 °C for 90 min. PVDF/TiO<sub>2</sub>/GO films were obtained by mixing PVDF/DMSO, GO/DMSO, and TiO<sub>2</sub>/DMSO solutions under sonication at 50 °C for 90 min. In all cases,

replace the liquid phase with DMSO. The colloidal suspension was then stirred for 30 min and sonicated for another 1 h to promote the dispersion of TiO<sub>2</sub> nanoparticles in DMSO.

was kept at 2.5 wt.% relative to the mass of TiO<sub>2</sub>.

the concentration of GO, TiO<sub>2</sub>, or GO+TiO<sub>2</sub> was kept constant at 2 wt.% relative to the total mass of the composite. The solutions were poured into Petri dishes and, after air-drying at 100 °C for 20 h, flexible self-supporting films were obtained after peeling them from the glassware. Fig. 1 shows a schematic of the experimental work performed in this study.

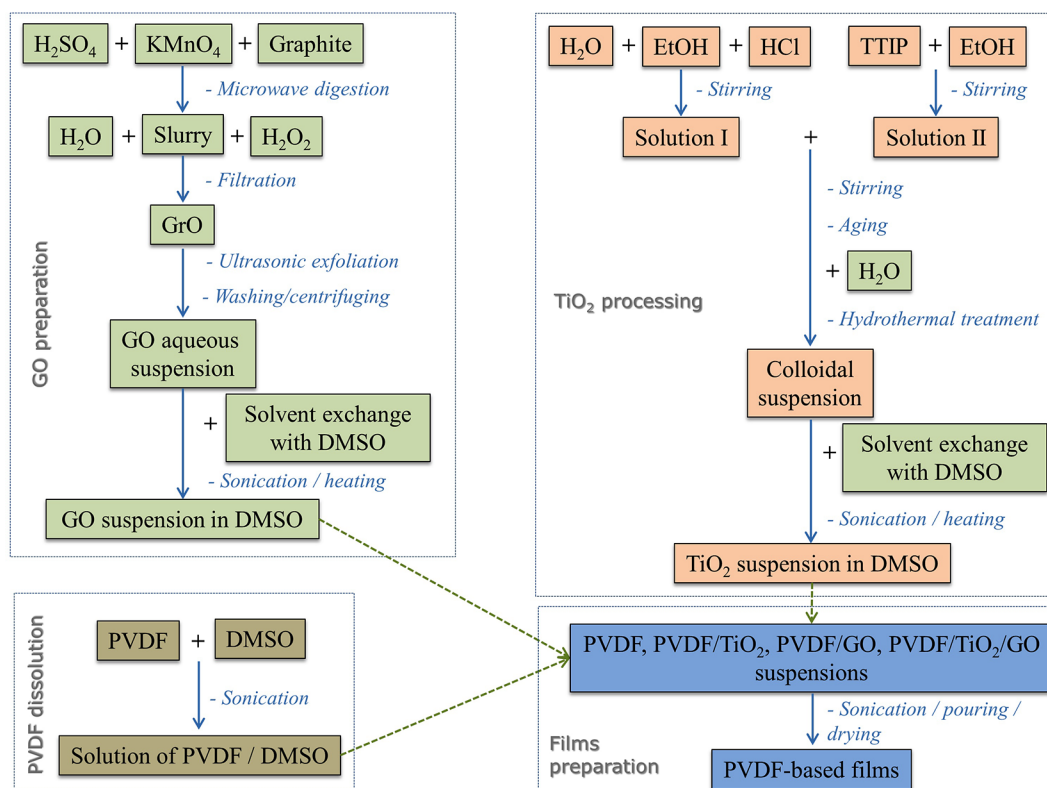


Figure 1 - Schematic of the experimental work performed in this study.

## 2.2. Characterizations

XRD was conducted on a Philips-PANalytical PW1710 diffractometer at a step size of 0.06° (2θ) and using CuKα (λ = 1.54 Å) as a radiation source. FTIR was performed on a Bruker Alpha spectrometer, using an attenuated total reflectance (ATR) accessory and a diamond crystal as the reflective element. These tests were carried out at a resolution of 4 cm<sup>-1</sup> and 128 scans. SEM was conducted

on an FEI Quanta 200 microscope at an accelerating voltage of 20 kV. The samples used in SEM were fixed on the stubs with a double-sided carbon tape and no coating step with a conductive layer was employed. AFM was performed on an Asylum Research MFP-3D microscope operating in the non-contact mode. A silicon cantilever with a spring constant of 26 N.m<sup>-1</sup> and resonance frequency of

30 kHz was employed in these tests. DSC was conducted on a TA Instruments Q10 series apparatus at heating/cooling rates of 10 °C.min<sup>-1</sup> under N<sub>2</sub> flow (50 mL.min<sup>-1</sup>). Two runs were performed for each sample, and the second run was taken into account in these examinations; such an approach is commonly used in literature to ensure the collection of more reproducible data. The wettability behavior was examined

by dripping deionized water (3  $\mu$ L) onto the prepared films and evaluating the contact angle of sessile droplets with the solid surface. These measurements were taken before and after exposing the films to UV-A light for either 90 min or 180 min. These irradiations were performed on a chamber equipped with

an 18 W lamp (Osram Dulux S Blue / maximum emission at 354 nm). The samples were kept 5 cm away from the UV A lamp and were ventilated with air to avoid heating. EIS was performed on a PGSTAT AUTOLAB 302 system using disc-shaped samples (0.05 mm thick and 1 cm<sup>2</sup> in area) pressed between

two steel electrodes. The frequency used ranged from 0.1 kHz to 10 kHz, while the amplitude of the sinusoidal input signal was kept constant at 0.1 V. Two steel electrodes were used to press the disc samples. An equivalent circuit was simulated with the Zview<sup>®</sup> software to interpret the data obtained.

### 3. Results

#### 3.1. Structural characterization

Fig. 2a displays XRD patterns taken for PVDF-based films prepared in this study. It appears that the orthorhombic  $\beta$ -phase of PVDF is the main crystalline phase in these materials, which is evidenced by the strong diffraction line at  $2\theta = 20.6^\circ$  assigned to (110) and (200) reflections (Cai *et al.*, 2017). As discussed before, this phase has the highest polarity among PVDF's phases due to a TTTT conformation. The  $\alpha$ -phase is also identified by the lines at  $2\theta = 18.4^\circ$ ,  $33.2^\circ$ ,  $35.9^\circ$ ,  $38.8^\circ$ , and  $41.1^\circ$ , which have been ascribed to (020), (130), (200), (002), and (111) reflections (Cai *et al.*, 2017). TiO<sub>2</sub>

anatase is observed in the TiO<sub>2</sub>-containing composites. According to the JCPDS card file N<sup>o</sup> 21-1272, the line at  $2\theta = 25.6^\circ$  is related to the (101) crystal plane of anatase. Indeed, it has been reported that the sol-gel route used here gives rise to TiO<sub>2</sub> anatase (Silva, L.M.C. *et al.*, 2021). It is also possible that the  $\alpha$ -phase of PVDF may contribute to this signal because it has a diffraction line ascribed to its (021) crystal plane at  $2\theta = 26.6^\circ$  (Cai *et al.*, 2017). Fig. 2b exhibits XRD patterns collected for GO-containing samples exposed to UV-A light for either 90 min or 180 min. No expressive changes in these patterns

were noticed, revealing that PVDF remained stable even after its exposition to UV-A radiation. The appearance of a broad hump centered at about  $25^\circ$  can be related to the reduction of GO into rGO (Hidayah *et al.*, 2017; Qiao *et al.*, 2015). This peak is more visible for the PVDF/GO sample exposed to UV-A light for 90 min than for 180 min. This behavior could be related to process variability, such as inhomogeneous illumination or heterogeneity in the prepared specimens. Additional crystalline phases of PVDF could not be resolved by XRD, which is why we also used FTIR spectroscopy.

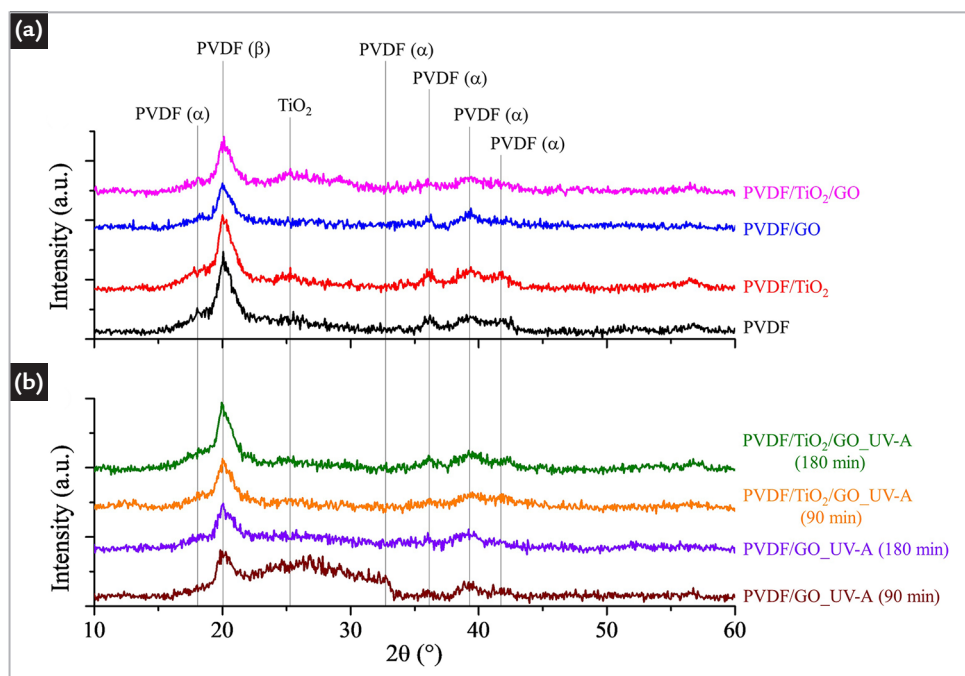


Figure 2 - XRD patterns taken for PVDF-based films prepared in this study, (a) before and (b) after irradiation with UV-A light for 90 min or 180 min.

Figs. 3a and 3b show the ATR-FTIR spectra of films before and after exposure to UV-A light. The absorption band at  $1430\text{ cm}^{-1}$  has been attributed to the bending mode of CH<sub>2</sub> groups and is commonly observed for all crystalline phases of PVDF (Boccaccio *et al.*, 2002). The distinction by FTIR between the  $\beta$ - and  $\gamma$ -phases is challenging due to their similar conforma-

tion. The bands at  $1400\text{ cm}^{-1}$ ,  $1234\text{ cm}^{-1}$ ,  $1160\text{ cm}^{-1}$ ,  $875\text{ cm}^{-1}$ ,  $836\text{ cm}^{-1}$ ,  $508\text{ cm}^{-1}$ ,  $475\text{ cm}^{-1}$ , and  $430\text{ cm}^{-1}$  have been associated with the  $\beta$ -phase. The bands at  $1275\text{ cm}^{-1}$  and  $1234\text{ cm}^{-1}$  can be due to the  $\gamma$ -phase. As mentioned before, this phase is hardly observed in PVDF samples. Nonetheless, it has been reported that GO (Mohamadi, Sharifi-Sanjani and Foyouhi,

2012) and TiO<sub>2</sub> (An *et al.*, 2011a) can favor the formation of the  $\gamma$ -phase in PVDF-based composites. The absorption bands at  $763\text{ cm}^{-1}$  and  $600\text{ cm}^{-1}$  have been attributed to the  $\alpha$ -phase. It appears that the  $\beta$ -phase is the main crystalline phase in the prepared samples, which is in line with XRD (Fig. 2). It has been reported that the lack of strong absorption bands assigned to

CF<sub>2</sub> molecules between about 650 cm<sup>-1</sup> to 800 cm<sup>-1</sup> suggests that the β-phase is the major crystalline phase in PVDF (Silva,

Liliane A *et al.*, 2019; Thakur *et al.*, 2023). Nonetheless, the α-phase also appears to be present in a considerable amount. No signifi-

cant change in the FTIR spectra was noticed after the UV-A irradiation of GO-containing specimens, which also agrees with XRD.

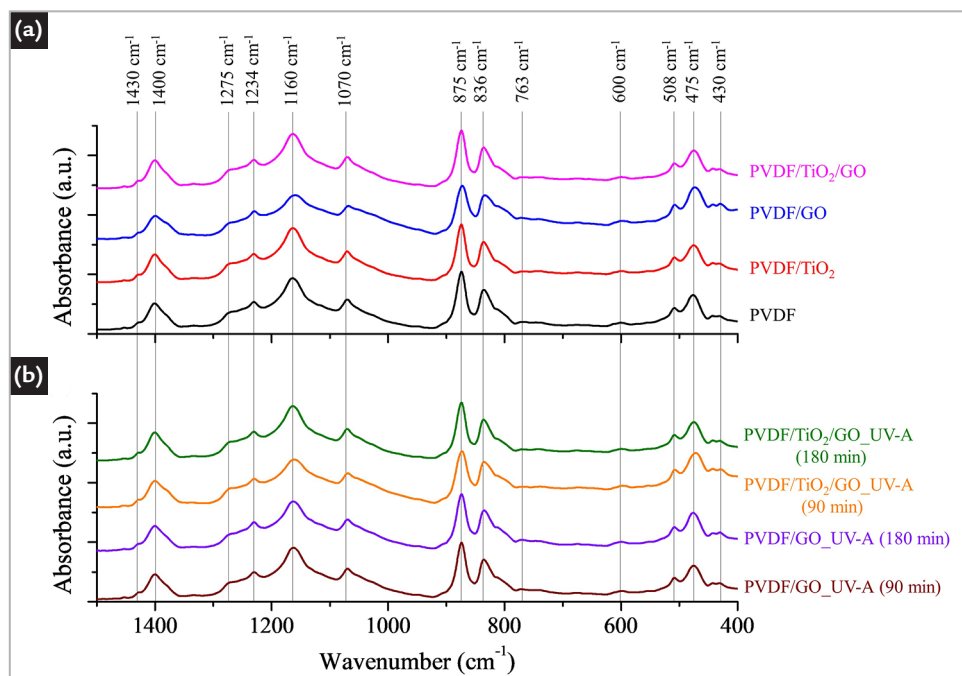


Figure 3 - ATR-FTIR spectra collected for PVDF-based films prepared in this study, (a) before and (b) after irradiation with UV-A light for 90 min or 180 min.

Figure 4 shows SEM micrographs of films prepared in this study. Spheroidal structures also called "spherulites" are observed in pure PVDF. These structures have been related to the α-phase (Jaleh & Jabbari, 2014) and are composed of small crystals that grow in a radial direction, with the formation of branches in three-dimensional space (Toda,; Arita, and Hikosaka, 2001). PVDF/TiO<sub>2</sub> has TiO<sub>2</sub> particles associated with PVDF spherulites, which is also evidenced in the composition map displayed. Ti is observed to be homogeneously dispersed in PVDF/TiO<sub>2</sub>, revealing that the mixture of the starting suspensions of PVDF and TiO<sub>2</sub> was successfully performed. It appears that the incorporation of GO into PVDF inhibits the formation of spherulites. The presence of carbonyl groups in GO and fluorine in PVDF has been reported to favor their interaction and restrict the formation of spherulites (Lu, Zuo and Chung, 2017; Viegas *et al.*, 2017). Such a finding appears more visible when GO and TiO<sub>2</sub> are co-added to PVDF as smoother films without spherulite are observed for PVDF/GO/TiO<sub>2</sub>. The strong interaction between surface OH groups present on TiO<sub>2</sub> and C-F bonds of the PVDF backbone could restrict the movement and arrangement of the

polymer chains, further inhibiting the formation of spherulites (An *et al.*, 2011b). TiO<sub>2</sub> particles are also observed for PVDF/TiO<sub>2</sub>/GO, which was already expected.

Figure 5 shows AFM images taken for these materials. The bright areas represent the highest points on the examined surface and the dark regions indicate valleys. Spherulites are observed for PVDF and PVDF/TiO<sub>2</sub>. Sharp peaks related to titania particles are noticed for samples containing TiO<sub>2</sub>. Table 1 brings the roughness parameters evaluated by AFM, considering a scanning area of about 5 μm × 5 μm. Ra is the roughness average, while Rq is the root mean square of a surface. The addition of TiO<sub>2</sub> to PVDF increased the roughness of the latter, which may be due to the presence of titania particles on the composite surface. Incorporating GO significantly increased the surface roughness of PVDF, which was also reported by other authors (Alkhouzaam & Qiblawey, 2021; Niu *et al.*, 2016). The strong interaction between GO and PVDF may favor their dispersion but inhibits the formation of spherulites and gives rise to rough surfaces. The co-addition of GO and TiO<sub>2</sub> to PVDF leads to surfaces with roughness much lower than that observed for PVDF/GO but

higher than that evaluated for PVDF. As evidenced in Figure 6, the exposure of these films to UV-A light increased their surface roughness. Sharp peaks are observed on the surface of PVDF/GO after its irradiation with UV-A light, and they become more noticeable after 180 min of exposure. These features may be due to defects induced by UV-A light in PVDF (Lee, Mei jiun *et al.*, 2016) and GO (YOON *et al.*, 2020). This effect was less pronounced for samples prepared by co-addition of TiO<sub>2</sub> and GO, probably because part of the incoming UV-A photons was absorbed by titania particles, shielding the polymer matrix and inhibiting the formation of defects on the irradiated films. TiO<sub>2</sub> anatase has a bandgap energy of 3.2 eV (Tang *et al.*, 1994), which means that incoming photons with wavelengths shorter than about 388 nm can be absorbed by it, resulting in the formation of electron-hole pairs. Absorption of UV-A photons by TiO<sub>2</sub> prevents them from reaching the polymer matrix, thereby protecting it from degradation. Similar behavior was also reported by Liu *et al.* (Liu, Zhanjian *et al.*, 2021). It is worth noting that no cracks or fractures were observed in the UV-A illuminated samples, even when exposure times of up to 180 min were used.

The Serra do Facão Hydroelectric Power Plant, located in the state of Goiás, Brazil, was selected as part of the study area in this research for the analysis of operational dispatch flows and identification of residual/

ecological flows. The historical series pertaining to the Serra do Facão Hydroelectric Power Plant was obtained via the Reservoir Monitoring System (SAR) maintained by ANA. According to information provided by the plant

administrators FURNAS (2020b) and SEFAC (2020), the Serra do Facão Hydroelectric Power Plant is a run-of-river type located on the São Marcos River. The characteristics of the plant are presented in Table 4.

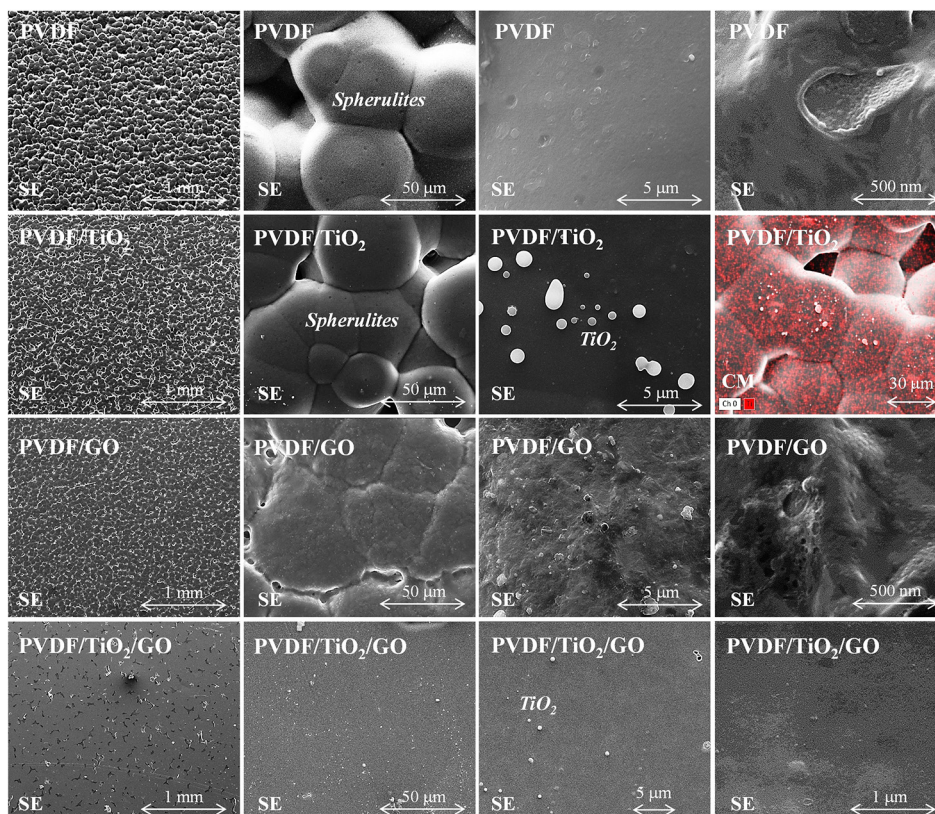


Figure 4 - SEM micrographs (secondary electrons – SE) and compositional map (EDS analysis – CM) obtained for PVDF-based films.

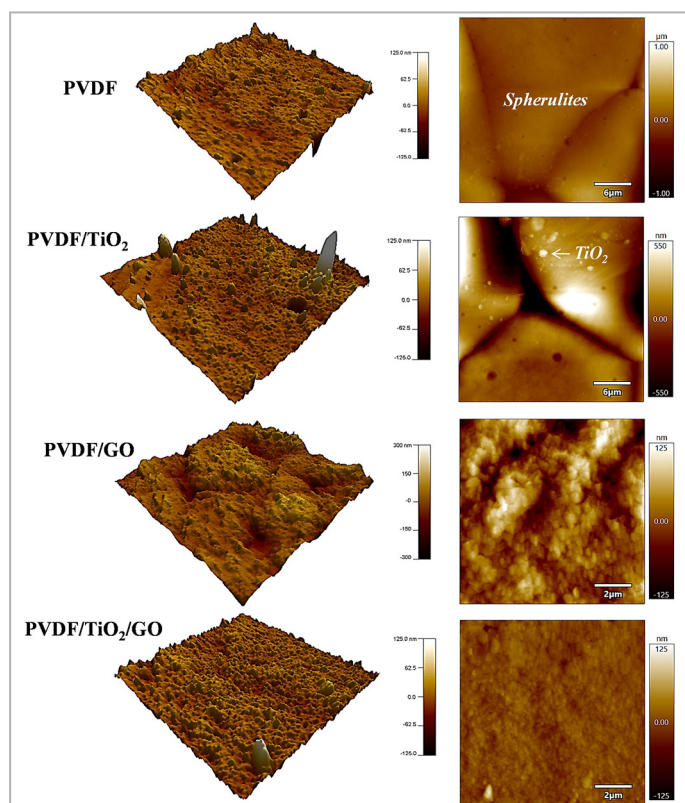


Figure 5 - 2D- and 3D-AFM images of PVDF-based films prepared in this study.

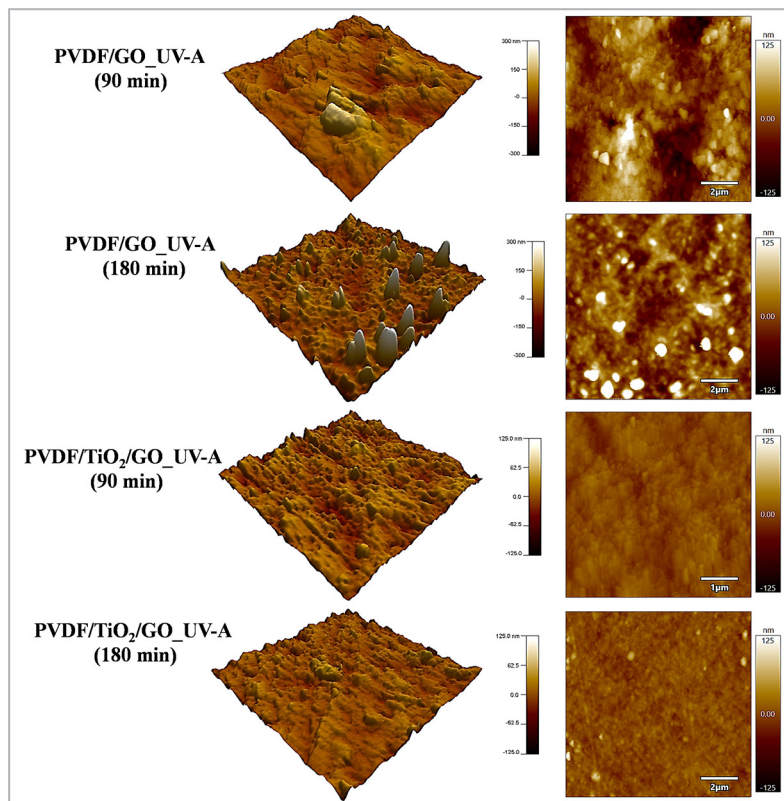


Figure 6 - 2D- and 3D-AFM images of PVDF-based films after exposure to UV-A light for 90 min or 180 min.

It has been reported that UV-A radiation promotes the degradation of hydrocarbons (RH) through the mechanisms of chain initiation, propagation, and termination described in Eq. (1) to (5) (Lee, Mei Jiun *et al.*, 2016). Eq. (1) expresses the formation of free radicals (R· and H·) during the UVA-irradiation of the polymer. The hydrocarbon radicals

(R·) generated could react with oxygen to form peroxy radicals (ROO·) (Eq. (2)) and also suppress hydrogen from the polymer chains. Such a reaction could lead to hydroperoxide radicals (ROOH) (Eq. (3)). The decomposition of these radicals may lead to the breaking of O-O bonds and a consequent scission of the polymer chain. The radical propagation can be

terminated when two radicals combine, which is represented by Eq. (4) and (5). The occurrence of these reactions causes a significant change in the polymer morphology (Rabek, 1995). Based on the results described so far, it can be assumed that PVDF was affected by UV A light and experienced the reactions described in Eq. (1) to (5).

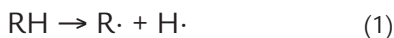


Table 1 - Roughness parameters evaluated by AFM.

Condition	Sample	Roughness	
		R <sub>a</sub> (nm)	R <sub>q</sub> (nm)
As-prepared	PVDF	7.5	11.2
	PVDF/TiO <sub>2</sub>	9.8	16.7
	PVDF/GO	27.6	35.1
	PVDF/TiO <sub>2</sub> /GO	8.8	13.2
UV-A irradiated	PVDF/GO_UV-A (90 min)	29.3	38.6
	PVDF/GO_UV-A (180 min)	29.4	41.9
	PVDF/TiO <sub>2</sub> /GO_UV-A (90 min)	10.1	13.9
	PVDF/TiO <sub>2</sub> /GO_UV-A (180 min)	8.2	12.0

Figure 7 displays the DSC profiles obtained in this study. An endothermic signal associated with the melting of PVDF was observed in the heating stage, while the exothermic peak noted in the cooling step is due to its crystallization. One observes that the addition of GO, TiO<sub>2</sub>, or GO+TiO<sub>2</sub> to

PVDF has affected both temperatures, namely T<sub>m</sub> (melting) and T<sub>c</sub> (crystallization). A broad melting peak has been observed for all samples due to multiple phases (Pickford *et al.*, 2019), which is also supported by XRD and FTIR (Figs. 1 and 2). Table 2 brings thermodynamic parameters evaluated

$$X_{\text{DSC}} = \frac{\Delta H_m}{\Delta H_0} \times 100 \quad (6)$$

PVDF displayed T<sub>m</sub> and T<sub>c</sub> equal to 166.5 °C and 136.4 °C. The specific latent melting heat and crystallization for this material was estimated at -45.4 J.g<sup>-1</sup> and 20.8 J.g<sup>-1</sup>, respectively. These values are in agreement with those reported elsewhere (Viegas *et al.*, 2017). Incorporating GO into PVDF has changed these values, increasing T<sub>m</sub> and T<sub>c</sub> to 172.4 °C and 141.1 °C. These changes were accompanied by an increase in ΔH<sub>m</sub> to 50.4 J.g<sup>-1</sup> and a decrease in ΔH<sub>c</sub> to 15.9 J.g<sup>-1</sup>. It has been reported that GO can act as an active site for heterogeneous nucleation, lowering the crystallization energy of PVDF and leading to the formation of β phase (Lee, Jung-Eun *et al.*, 2019). Adding TiO<sub>2</sub> to PVDF caused an increase in ΔH<sub>m</sub> and ΔH<sub>c</sub> to 50.8 J.g<sup>-1</sup> and 21.2 J.g<sup>-1</sup>. It has been already reported that the incorporation of inorganic metal

salts such as NaCl and LiBF<sub>4</sub> into the PVDF matrix favors the formation of the β-phase (Tiwari & Maiti, 2023). PVDF/GO and PVDF/TiO<sub>2</sub> displayed crystallinity of about 48%, which was higher than that assessed for pure PVDF (about 43%). On the other hand, the co-addition of GO and TiO<sub>2</sub> to PVDF led to a composite with a lower crystallinity (about 42%), in addition to smaller ΔH<sub>m</sub> and ΔH<sub>c</sub> (-43.7 J.g<sup>-1</sup> and 19.2 J.g<sup>-1</sup>, respectively). As mentioned before, it appears that the strong interaction observed for PVDF, GO, and TiO<sub>2</sub> inhibits the movement and alignment of the polymer chains, leading to less-ordered structures. Similar behavior has been reported by other authors (Rekik *et al.*, 2013).

The UV-A irradiation of GO-containing composites caused a change in

these thermodynamic parameters. They were more visible for PVDF/GO, revealing that UV A radiation greatly affected this material. It has been reported that radiation-induced defects in PVDF cause a dramatic change in T<sub>m</sub>, which is in agreement with this study (Viegas *et al.*, 2017). On the other hand, PVDF/TiO<sub>2</sub>/GO was less affected, suggesting that it has a high resistance to UV-A light. This result is in line with Figure 6, where fewer radiation-induced defects are observed for this composite. As mentioned before, it appears that TiO<sub>2</sub> partially protects the polymer matrix, thus inhibiting the formation of defects in it. This higher UV-A light resistance observed for the TiO<sub>2</sub>-containing composites deserves to be highlighted and suggests a potential use of these materials in UV protection devices.

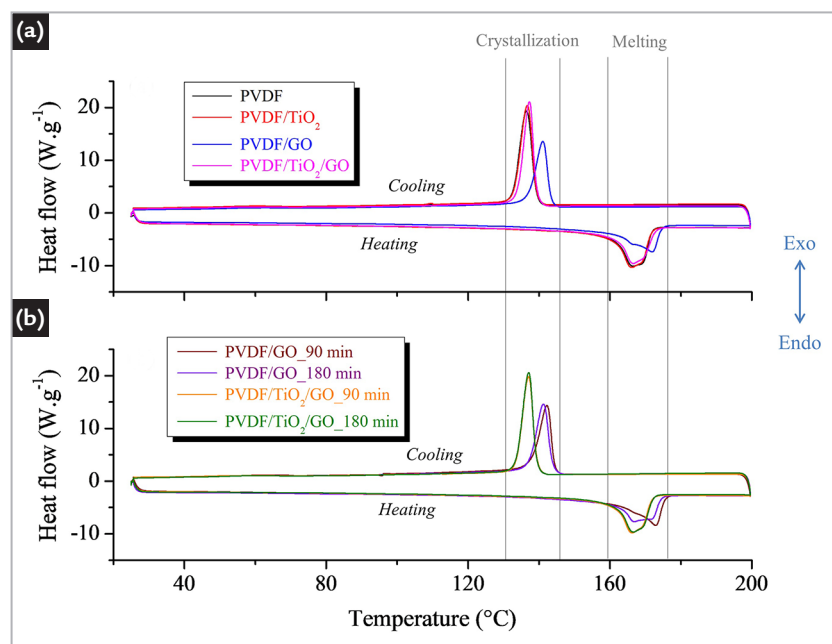


Figure 7 - DSC profiles obtained for the samples prepared in this study. Two runs were conducted for each sample, and the second cycle was considered. The reader is encouraged to consult the online version of the manuscript to see these curves in color.

The production of materials with improved UV-A light resistance may have several potential applications, including exterior coatings, as the TiO<sub>2</sub>-containing

composites could be used as a protective coating on exterior surfaces, such as building facades, roofs, and bridges to prevent degradation from UV radiation and

weathering. In addition, these materials have potential applications as protective coatings for batteries and other energy storage devices to prevent UV-A-induced

degradation and extend their life, and for medical devices, as these composites could be used in the development of medical

devices that require high UV-A resistance, such as implants and prosthetics. In electronics, these composites could be used as

a protective coating for electronic devices, such as sensors to prevent damage from UV radiation.

Table 2 - Thermodynamic parameters obtained from the DSC curves exhibited in Figure 7.

Condition	Sample	$T_m$ (°C)	$\Delta H_m$ (J.g <sup>-1</sup> )	$X_{dsc}$ (%)	$T_c$ (°C)	$\Delta H_c$ (J.g <sup>-1</sup> )
As-prepared	PVDF	166.5	-45.4	43.3	136.4	20.8
	PVDF/TiO <sub>2</sub>	166.4	-50.8	48.3	136.8	21.2
	PVDF/GO	172.4	-50.4	48.0	141.1	15.9
	PVDF/TiO <sub>2</sub> /GO	166.8	-43.7	41.6	137.3	19.2
UV-A irradiated	PVDF/GO UV-A (90 min)	172.6	-46.2	44.0	142.2	18.3
	PVDF/GO UV-A (180 min)	167.0	-46.5	44.3	141.2	17.8
	PVDF/TiO <sub>2</sub> /GO UV-A (90 min)	166.4	-47.0	44.8	137.0	18.7
	PVDF/TiO <sub>2</sub> /GO UV-A (180 min)	166.6	-46.9	44.6	137.0	19.3

### 3.2 Wettability behavior

The wettability behavior of the prepared films is exhibited in Figure 8. The addition of TiO<sub>2</sub> to PVDF led to self-supporting films with a smaller water contact angle ( $81.5 \pm 3.3^\circ$  versus  $72.7 \pm 3.8^\circ$ ). Titania usually has a high concentration of hydrophilic groups on its surface, which could contribute to the wettability behavior of PVDF/TiO<sub>2</sub> (Safarpour, Khataee and Vatanpour, 2014, 2015). Blending PVDF with GO or GO+TiO<sub>2</sub> gave rise to specimens with contact angles similar to PVDF, namely  $80.2 \pm 3.6^\circ$  and  $81.5 \pm 3.3^\circ$ . On the one hand, the UV-A illumination of GO-

containing films for 90 min caused these contact angles to decrease; the values found for PVDF/GO and PVDF/TiO<sub>2</sub>/GO were  $65.9 \pm 6.5^\circ$  and  $79.1 \pm 2.3^\circ$ , respectively. On the other hand, extending the illumination time to 180 min caused an increase in the contact angle to  $79.1 \pm 2.3^\circ$  (PVDF/GO) and  $87.3 \pm 2.7^\circ$  (PVDF/TiO<sub>2</sub>/GO). rGO is reported to be hydrophobic due to the removal of oxygen functional groups from GO during the photoreduction step (Some *et al.*, 2013), which could contribute to the higher wetting angle observed for the UV-A irradiated samples. Moreover,

the removal of hydrophilic hydroxyl groups from TiO<sub>2</sub> takes place during UV-A illumination, thus contributing to the hydrophobic behavior observed for the TiO<sub>2</sub>-containing samples. It is worth mentioning that the UV-A illumination of pure PVDF did not cause any statistical change in its wetting angle, remaining stable at about  $82.2 \pm 3.6^\circ$ . However, PVDF/TiO<sub>2</sub> experienced a more dramatic change in its wettability behavior after UV-A irradiation, and the contact angle increased from  $72.7 \pm 3.8^\circ$  to  $85.6 \pm 2.4^\circ$  (90 min) and  $88.1 \pm 5.6^\circ$  (180 min).

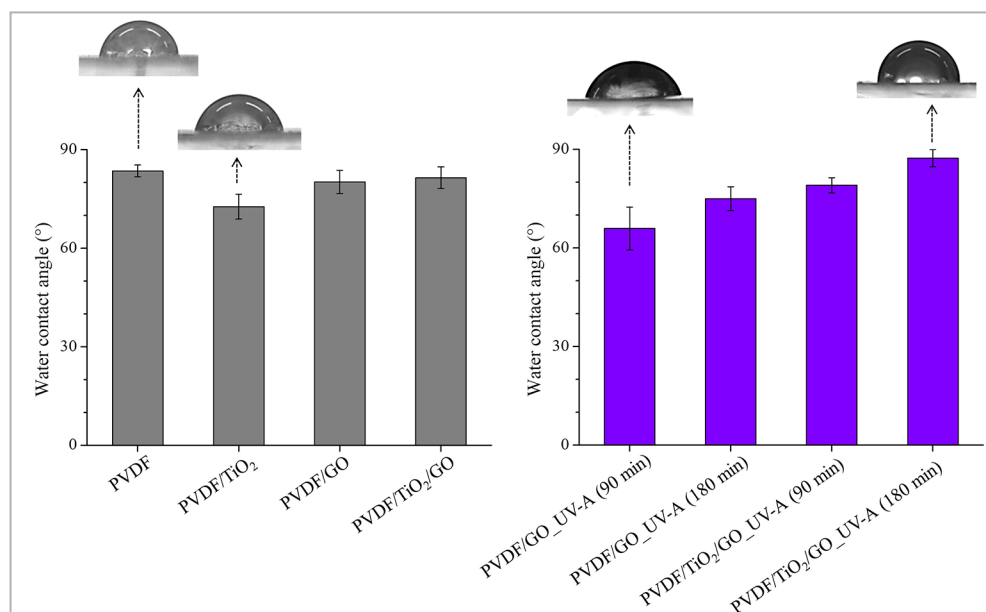


Figure 8 - Contact angle evaluated for sessile water droplets deposited on PVDF-based films prepared in this study. Inset: photograph of water droplets dripped onto the examined substrates. The contact angle evaluated for pure PVDF remained stable at about  $82.2 \pm 3.6^\circ$  after the irradiation with UV-A light.

### 3.3 Electrical properties

Figure 9a shows Nyquist plots for self-supporting films obtained in this

study. An equivalent electrical circuit was also simulated to support the discussion

of these results (inset in Fig. 9a). One observes that the examined materials

displayed similar behavior. The electronic resistance of the polymeric matrix and the contact resistance between the components are observed in the high-frequency region (Abdulkhaleem *et al.*, 2014). A semicircle associated with a charge transfer process and the capacitive behavior of the examined samples is also observed in these curves (Sengwa, Choudhary and Sankhla, 2010). Since PVDF is a dielectric material, the accumulation of charge carriers at the electrode/film interface is expected due to the polarization of the steel electrode. This behavior leads to the formation of an electrical double layer at this interface and leads to the semicircles observed in the EIS curves. In the proposed equivalent circuit, R represents the electrical resistance of the polymer matrix, Z<sub>w</sub> is the so-called Warburg impedance, while R<sub>ct</sub> and C<sub>dl</sub> are the charge transfer resistance and double layer capacity observed at the electrode/film interface. Pure PVDF showed the highest electrical resistance, which is evidenced by the large radius of the semicircle observed. This is because PVDF inhibits charge transfer through its matrix, which is called electrochemical inactivity and is commonly observed for polymers (Huang *et al.*, 2013; Qiu *et al.*, 2015).

The addition of either TiO<sub>2</sub> or GO to PVDF caused a decrease in the semicircle radius, revealing that the

obtained composites exhibit higher electrical conductivity than pure PVDF. In the case of PVDF/GO, a sharp decrease in the electrical resistance is observed due to the interconnected conducting network of graphene (Ren *et al.*, 2012). On the other hand, PVDF/TiO<sub>2</sub>/GO showed low charge transfer capacity, which is probably due to poor contact between the electrically active particles. Such behavior could be improved, for instance, by increasing the Lewis acid-base interactions between the TiO<sub>2</sub> particles and polymer chains, thus providing more pathways for charge transfer through the composite (Khasi, Youssefi and Semnani, 2020). In addition, one should consider that surface roughness also plays a key role in electrical conductivity (Javidjam *et al.*, 2018); the smoother surface observed for PVDF/TiO<sub>2</sub>/GO (Figs. 3 and 4) may also have contributed to this behavior. Rekik *et al.* (2013) investigated the dielectric relaxation behavior of PVDF/TiO<sub>2</sub> nanocomposites by broadband dielectric spectroscopy, and three relaxation processes have been reported. The first one occurred at about -40 °C and 10 Hz, and was attributed to the glass transition at low temperatures. The second phenomenon, which occurred at 30 °C and 10 Hz, is related to dipolar relaxations in the crystalline phase. The third one, at 100 °C and 10 Hz, was associated with an interfacial po-

larization. The crystallinity decreased and the electric modulus of interfacial polarization increased with increasing the TiO<sub>2</sub> content. It was reported that the interparticle distances reduce as the filler concentration increases, which can also result in an overlap of immobile polymer regions around the nanoparticle. It is possible that the so-called Maxwell-Wagner-Sillars effect can take place in the composite system studies in this research, especially for PVDF/TiO<sub>2</sub>/GO. Such an effect has been assigned to be due to the accumulation of charge carriers at the interfaces of heterogeneous systems (Rahimabady *et al.*, 2013; Xu *et al.*, 2015).

Exposing the GO-containing samples to UV-A light caused an increase in electrical conductivity, which is evidenced by the reduction in semicircle size (Figure 9b). This can be due to the photo-assisted reduction of GO into rGO upon UV-A illumination. It has been reported that rGO has no bandgap and higher electrical conductivity than GO (Gonçalves; Palhares; *et al.*, 2019). This reduction was more visible for PVDF/GO than for PVDF/TiO<sub>2</sub>/GO. As mentioned before, it appears that the TiO<sub>2</sub> particles could have inhibited the exposure of PVDF and GO to UV A light, causing a partial shielding of the polymer phase. This behavior could compromise GO photoreduction and inhibit rGO formation.

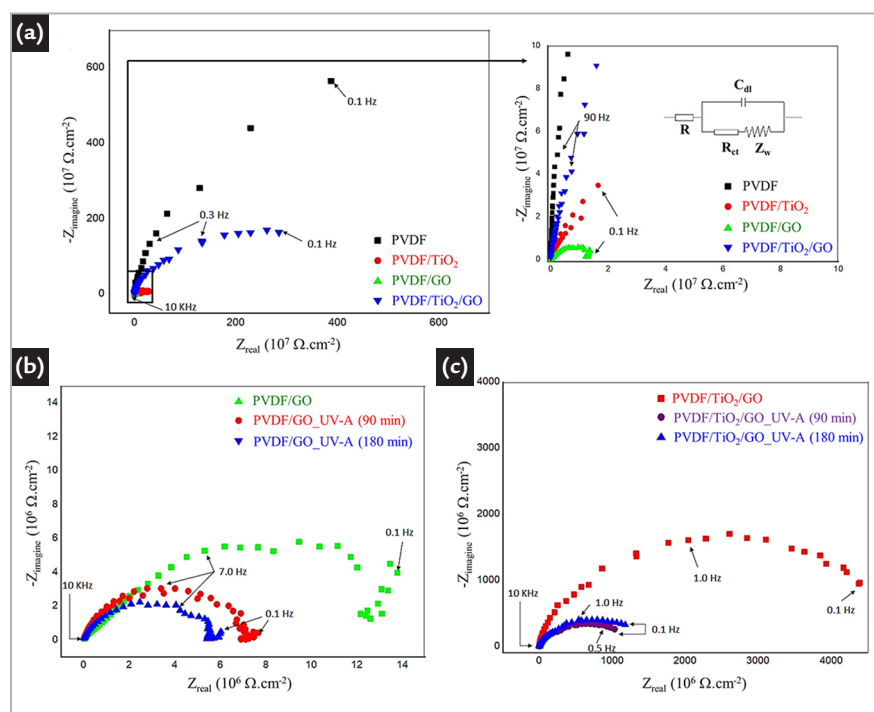


Figure 9 - EIS spectra collected for the PVDF-based films prepared in this study (a) before and (b) after exposure to UV-A light for either 90 min or 180 min. Inset: equivalent electrical circuit simulated for the examined specimens.

## 4. Conclusions

In this study, we have successfully prepared self-supporting, flexible and lightweight PVDF-based films using DMSO as a solvent. DMSO is an inexpensive and environmentally friendly solvent, which adds to the versatility of the proposed route. These materials were prepared by a simple route based on mixing and air drying PVDF, GO and TiO<sub>2</sub> suspensions.  $\beta$ -PVDF is the major phase in the prepared samples as evidenced by XRD and FTIR. Spheroidal structures typical of PVDF were observed for pure PVDF and PVDF/TiO<sub>2</sub>. Incorporation of GO (2 wt.%) into PVDF inhibited the formation of such structures, which was attributed to the strong interaction

between GO nanosheets and PVDF chains, preventing PVDF from crystallizing. Smooth films were prepared after co-addition of TiO<sub>2</sub> and GO to PVDF, in which no spherulite was observed. The structural changes induced by the addition of GO and TiO<sub>2</sub> to PVDF were accompanied by a change in  $T_m$ ,  $T_c$ ,  $\Delta H_m$  and  $\Delta H_c$ . Such changes are related to the strong interaction of the polymer chains with GO and TiO<sub>2</sub>, which affect their mobility and inhibit PVDF crystallization. Exposure of PVDF/GO to UV-A light caused a dramatic formation of defects on their surface, as evidenced by AFM. On the other hand, the TiO<sub>2</sub>-containing composites showed high resistance to UV-A

light, which may be due to the shielding effect promoted by the anatase particles; incoming UV-A photons could be absorbed by TiO<sub>2</sub>, leading to the formation of electron-hole pairs in it and causing this shielding effect. The high UV-A resistance of the prepared composites should be highlighted, as it allows them to be used in applications where high solar irradiances are observed. EIS tests showed that the addition of either GO or TiO<sub>2</sub> to PVDF caused a decrease in the electrical resistivity of the latter. However, the co-addition of GO and TiO<sub>2</sub> to PVDF resulted in samples with low charge transfer capacity, probably due to poor contact between the electrically active particles.

## Acknowledgements

The authors thank the financial support from CAPES (PROEX), CNPq (306193/2020 and 403191/2021-1),

and FAPEMIG (APQ-00792-17). We also thank the technical support from the UFMG microscopy center,

Samuel Lima, Prof. Vicente Buono, Prof. Andréia Bicalho, and Prof. Paulo Brandão.

## References

- ABDELMAKSOU, M. *et al.* Physical properties of PVDF-GO/black-TiO<sub>2</sub> nanofibers and its photocatalytic degradation of methylene blue and malachite green dyes. *Environmental Science and Pollution Research*, v. 28, p. 30613-30625, 2021.
- ABDULHAKEEM, B. *et al.* Morphological characterization and impedance spectroscopy study of porous 3D carbons based on graphene foam-PVA/phenol-formaldehyde resin composite as an electrode material for supercapacitors. *RSC Advances*, v. 4, p. 39066-39072, 2014.
- ALKHOUZAAM, A.; QIBLAWEY, H. Synergetic effects of dodecylamine-functionalized graphene oxide nanoparticles on antifouling and antibacterial properties of polysulfone ultrafiltration membranes. *Journal of Water Process Engineering*, v. 42, p. 102-120, 2021.
- ALTOMARE, A.; LOOS, K. Metal-free atom transfer radical polymerization of PVDF-based block copolymers catalyzed by organic photoredox catalysts. *Macromolecular Chemistry and Physics*, v. 224, n. 1, p. 2200259, 2023.
- AN, N. *et al.* Preparation and electroactive properties of a PVDF/nano-TiO<sub>2</sub> composite film. *Applied Surface Science*, v. 257, p. 3831-3835, 2011.
- ATHANASEKOU, C. *et al.* Mixed matrix PVDF/Graphene and composite-skin PVDF/Graphene Oxide membranes applied in membrane distillation. *Polymer Engineering & Science*, v. 59, p. E262-E278, 2019.
- BOCCACCIO, T. *et al.* Characterization of PVDF membranes by vibrational spectroscopy. *Journal of Membrane Science*, v. 210, p. 315-329, 2002.
- BOSC, F.; AYRAL, A.; GUIZARD, C.. Mesoporous anatase coatings for coupling membrane separation and photocatalyzed reactions. *Journal of Membrane Science*, v. 265, p. 13-19, 2005.
- CAI, X. *et al.* A critical analysis of the  $\alpha$ ,  $\beta$  and  $\gamma$  phases in poly(vinylidene fluoride) using FTIR. *RSC Advances*, v. 7, p. 15382-15389, 2017.
- CASTRO, V. G. *et al.* *Process for obtaining graphite oxide and graphene oxide*: Products and uses. Brazilian patent n° 102016005632-2 A2, 2017.
- CHUA, C.K.; PUMERA, M. Chemical reduction of graphene oxide: a synthetic chemistry viewpoint. *Chemical Society Reviews*, v. 43, p. 291-312, 2014.
- CORREIA, H. M. G.; RAMOS, M. M. D. Quantum modelling of poly(vinylidene fluoride). *Computational Materials Science*, v. 33, p. 224-229, 2005.
- DE SILVA, K.K.H. *et al.* Chemical reduction of graphene oxide using green reductants. *Carbon*, v. 119, p. 190-199, 2017.
- DU, Jinying *et al.* Enhanced antifouling performance of ZnS/GO/PVDF hybrid membrane by improving hydrophilicity and photocatalysis. *Polymers for Advanced Technologies*, v. 30, p. 351-359, 2019.
- GOMES, J. *et al.* Influence of the  $\beta$ -phase content and degree of crystallinity on the piezo-and ferroelectric properties of poly(vinylidene fluoride). *Smart Materials and Structures*, v. 19, p. 065010, 2010.

- GONÇALVES, Bruno S.; PALHARES, Hugo G.; *et al.* Effect of the carbon loading on the structural and photocatalytic properties of reduced graphene oxide-TiO<sub>2</sub> nanocomposites prepared by hydrothermal synthesis. *Journal of Materials Research and Technology*, v. 8, n. 6, p. 6262-6274, 2019.
- GONÇALVES, Bruno S.; SOUZA, Tarcizo C.C. de; *et al.* Solvent effect on the structure and photocatalytic behavior of TiO<sub>2</sub>-RGO nanocomposites. *Journal of Materials Research*, v. 34, n. 23, p. 3918-3930, 2019.
- HANAOR, D. A. H.; SORRELL, C. C. Review of the anatase to rutile phase transformation. *Journal of Materials Science*, v. 46, n. 4, p. 855-874, 2011.
- HIDAYAH, N. M. S. *et al.* Comparison on graphite, graphene oxide and reduced graphene oxide: synthesis and characterization. *AIP Conference Proceedings*, v. 1892, p. 150002, 2017.
- HU, X. *et al.* Beaded electrospun polyvinylidene fluoride (PVDF) membranes for membrane distillation (MD). *Journal of Membrane Science*, v. 661, 2022.
- HUANG, Xiao-Lei *et al.* Homogeneous CoO on graphene for binder-free and ultralong-life lithium ion batteries. *Advanced Functional Materials*, v. 23, p. 4345-4353, 2013.
- JAKHAR, R.; YAP, J. E.; JOSHI, R. Microwave reduction of graphene oxide. *Carbon*, v. 170, p. 277-293, 2020.
- JALEH, B.; JABBARI, A. Evaluation of reduced graphene oxide/ZnO effect on properties of PVDF nanocomposite films. *Applied Surface Science*, v. 320, p. 339-347, 2014.
- JAVIDJAM, A. *et al.* Effect of surface roughness on electrical conductivity and hardness of silver plated copper. *Materials Research Express*, v. 6, p. 36407, 2018.
- KABIR, E. *et al.* Pure  $\beta$ -phase formation in polyvinylidene fluoride (PVDF)-carbon nanotube composites. *Journal of Physics D: Applied Physics*, v. 50, p. 163002, 2017.
- KARIMI, A. *et al.* The effect of different solvents on the morphology and performance of the ZIF-8 modified PVDF ultrafiltration membranes. *Separation and Purification Technology*, v. 253, p. 117548, 2020.
- KHASSI, K.; YOUSSEFI, M.; SEMNANI, D.. PVDF/TiO<sub>2</sub>/graphene oxide composite nanofiber membranes serving as separators in lithium-ion batteries. *Journal of Applied Polymer Science*, v. 137, p. 48775, 2020.
- LEE, Jung-Eun *et al.* Effect of interfacial interaction on the conformational variation of poly(vinylidene fluoride) (PVDF) chains in PVDF/graphene oxide (GO) nanocomposite fibers and corresponding mechanical properties. *ACS Applied Materials & Interfaces*, v. 11, p. 13665-13675, 2019.
- LEE, M.J. *et al.* Degradation of PVDF-based composite membrane and its impacts on membrane intrinsic and separation properties. *Journal of Polymer Engineering*, v. 36, p. 261-268, 2016.
- LIU, L. *et al.* Photocatalytic CO<sub>2</sub> reduction with H<sub>2</sub>O on TiO<sub>2</sub> nanocrystals: Comparison of anatase, rutile, and brookite polymorphs and exploration of surface chemistry. *ACS Catalysis*, v. 2, n. 8, p. 1817-1828, 2012.
- LIU, Zhanjian *et al.* Durable superhydrophobic PVDF/FEVE/GO@TiO<sub>2</sub> composite coating with excellent anti-scaling and UV resistance properties. *Chemical Engineering Journal*, v. 411, p. 128632, 2021.
- LU, K.-J.; ZUO, J.; CHUNG, T.-S.. Novel PVDF membranes comprising n-butylamine functionalized graphene oxide for direct contact membrane distillation. *Journal of Membrane Science*, v. 539, p. 34-42, 2017.
- MAHANTY, B. *et al.* Human skin interactive self-powered piezoelectric e-skin based on PVDF/MWCNT electrospun nanofibers for non-invasive health care monitoring. *Materials Today: Proceedings*, v. 21, p. 1964-1968, 2020.
- MARRA, M. *et al.* Structural and photocatalytic properties of sol-gel-derived TiO<sub>2</sub> samples prepared by conventional and hydrothermal methods using a low amount of water. *Journal of Sol-Gel Science and Technology*, 2022.
- MCKIM, Artie S.; STRUB, Robert. Dimethyl Sulfoxide USP, PhEur in approved pharmaceutical products and medical devices. *Pharmaceutical Technology*, v. 32, n. 5, 2008.
- MIKI, H. *et al.* Lithographic micropatterning on the  $\beta$ -PVDF film using reactive ion etching aim for high-resolution skin sensors. *IEEE Transactions on Electrical and Electronic Engineering*, v. 14, p. 1575-1577, 2019.
- MOHAMADI, S.; SHARIFI-SANJANI, N.; FOYOUHI, A. Evaluation of graphene nanosheets influence on the physical properties of PVDF/PMMA blend. *Journal of Polymer Research*, v. 20, p. 46, 2012.
- MOHAMAT, R. *et al.* Effect of surfactants' tail number on the PVDF/GO/TiO<sub>2</sub>-based nanofiltration membrane for dye rejection and antifouling performance improvement. *International Journal of Environmental Research*, v. 15, p. 149-161, 2021.
- NIU, Z. *et al.* Observations of atmospheric  $\Delta^{14}\text{CO}_2$  at the global and regional background sites in China: Implication for fossil fuel CO<sub>2</sub> inputs. *Environmental Science & Technology*, v. 50, n. 22, p. 12122-12128, 2016.
- PALHARES, H. G.; NUNES, E. H. M.; HOUMARD, M. Heat treatment as a key factor for enhancing the photodegradation performance of hydrothermally-treated sol-gel TiO<sub>2</sub>-SiO<sub>2</sub> nanocomposites. *Journal of Sol-Gel Science and Technology*, v. 99, p. 188-197, 2021.
- PALWAI, S. *et al.* Electrospun polyvinylidene fluoride nanofiber membrane-based flexible capacitive tactile sensors for biomedical applications. *Surface Engineering and Applied Electrochemistry*, v. 58, p. 194-201, 2022.
- PICKFORD, T. *et al.* Effects of an ionic liquid and processing conditions on the  $\beta$ -polymorph crystal formation in polyvinylidene fluoride. *CrystEngComm*, v. 21, p. 5418-5428, 2019.
- PIEDRAHITA-BELLO, M. *Fabrication of spin crossover nanocomposites and devices for electromechanical applications*. Université Paul Sabatier - Toulouse III, 2020.
- QIAO, X. *et al.* Phosphorus and nitrogen dual doped and simultaneously reduced graphene oxide with high surface area as efficient metal-free electrocatalyst for oxygen reduction. *Catalysts*, v. 5, p. 981-991, 2015.

- QIU, H. *et al.* In situ synthesis of GeO<sub>2</sub>/reduced graphene oxide composite on Ni foam substrate as a binder-free anode for high-capacity lithium-ion batteries. *Journal of Materials Chemistry A*, v. 3, p. 1619-1623, 2015.
- RABEK, J.F. *Polymer photodegradation: mechanisms and experimental methods*. Dordrecht: Springer Netherlands, 1995.
- RAHIMABADY, M. *et al.* Dielectric behaviors and high energy storage density of nanocomposites with core-shell BaTiO<sub>3</sub>@TiO<sub>2</sub> in poly(vinylidene fluoride-hexafluoropropylene). *Phys. Chem. Chem. Phys.*, v. 15, p. 16242-16248, 2013.
- REKIK, H. *et al.* Dielectric relaxation behaviour in semi-crystalline polyvinylidene fluoride (PVDF)/TiO<sub>2</sub> nanocomposites. *Composites Part B: Engineering*, v. 45, p. 1199-1206, 2013.
- REN, H. M. *et al.* Flexible free-standing TiO<sub>2</sub>/graphene/PVDF films as anode materials for lithium-ion batteries. *Applied Surface Science*, v. 263, p. 54-57, 2012.
- RUSSO, F. *et al.* Innovative poly(vinylidene fluoride) (PVDF) electrospun nanofiber membrane preparation using DMSO as a low toxicity solvent. *Membranes*, v. 10, 2020.
- SAFARPOUR, M.; KHATAEE, A.; VATANPOUR, V. Effect of reduced graphene oxide/TiO<sub>2</sub> nanocomposite with different molar ratios on the performance of PVDF ultrafiltration membranes. *Separation and Purification Technology*, v. 140, p. 32-42, 2015.
- SAFARPOUR, M.; KHATAEE, A.; VATANPOUR, V. Preparation of a novel polyvinylidene fluoride (PVDF) ultrafiltration membrane modified with reduced graphene oxide/titanium dioxide (TiO<sub>2</sub>) nanocomposite with enhanced hydrophilicity and antifouling properties. *Industrial & Engineering Chemistry Research*, v. 53, p. 13370-13382, 2014.
- SAXENA, P.; SHUKLA, P. A comprehensive review on fundamental properties and applications of poly(vinylidene fluoride) (PVDF). *Advanced Composites and Hybrid Materials*, v. 4, p. 8-26, 2021.
- SENGWA, R. J.; CHOUDHARY, S.; SANKHLA, S. Dielectric properties of montmorillonite clay filled poly(vinyl alcohol)/poly(ethylene oxide) blend nanocomposites. *Composites Science and Technology*, v. 70, p. 1621-1627, 2010.
- SILVA, L.M.C. *et al.* Preparation of titania-reduced graphene oxide composite coatings with electro- and photosensitive properties. *Applied Surface Science*, v. 538, p. 148029, 2021.
- SILVA, L. A *et al.* Enhancement of X-ray shielding properties of PVDF/BaSO<sub>4</sub> nanocomposites filled with graphene oxide. *MRS Advances*, v. 4, n. 3-4, p. 169-175, 2019.
- SOME, S. *et al.* Highly sensitive and selective gas sensor using hydrophilic and hydrophobic graphenes. *Scientific Reports*, v. 3, p. 1868, 2013.
- TANG, H. *et al.* Electrical and optical properties of TiO<sub>2</sub> anatase thin films. *Journal of Applied Physics*, v. 75, n. 4, p. 2042-2047, 1994.
- THAKUR, A. *et al.* Enhanced dielectric constant with addition of a low amount of SnO<sub>2</sub> nanoparticles as fillers in a PVDF matrix with low dielectric loss. *Nano-Structures & Nano-Objects*, v. 34, p. 100978, 2023.
- THAMIZHLARASAN, A. *et al.* Synthesis and characterization of functionalized polyvinylidene fluoride (PVDF) and the high temperature catalytic activity of PVDF-g-MAH/V<sub>2</sub>O<sub>5</sub> nanocomposite toward transesterification reaction. *Polymer Engineering & Science*, v. 62, p. 3010-3025, 2022.
- TIWARI, S.; MAITI, P. Salts induced piezoelectric effect in electrospun PVDF based nanohybrids for efficient energy harvesting. *Nano-Structures & Nano-Objects*, v. 33, p. 100945, 2023.
- TODA, A.; ARITA, T.; HIKOSAKA, M. Three-dimensional morphology of PVDF single crystals forming banded spherulites. *Polymer*, v. 42, p. 2223-2233, 2001.
- VIEGAS, J. *et al.* Increased X-ray attenuation efficiency of graphene-based nanocomposite. *Industrial and Engineering Chemistry Research*, v. 56, p. 11782-11790, 2017.
- WANG, X. *et al.* Tactile-sensing based on flexible PVDF nanofibers via electrospinning: a review. *Sensors*, v. 18, p. 330, 2018.
- XU, N. *et al.* Significantly enhanced dielectric performance of poly(vinylidene fluoride-co-hexafluoropropylene)-based composites filled with hierarchical flower-like TiO<sub>2</sub> particles. *ACS Applied Materials & Interfaces*, v. 7, p. 27373-27381, 2015.
- YIN, J.-Y. *et al.* Effects of solvent and electrospinning parameters on the morphology and piezoelectric properties of PVDF nanofibrous membrane. *Nanomaterials*, v. 12, p. 962, 2022.
- YOON, Y. *et al.* Comparing graphene oxide and reduced graphene oxide as blending materials for polysulfone and polyvinylidene difluoride membranes. *Applied Sciences*, v. 10, p. 1-10, 2020.
- ZHANG, J. *et al.* New understanding of the difference of photocatalytic activity among anatase, rutile and brookite TiO<sub>2</sub>. *Physical Chemistry Chemical Physics*, v. 16, p. 20382-20386, 2014.

---

Received: 3 June 2023 - Accepted: 10 October 2023.



All content of the journal, except where identified, is licensed under a Creative Commons attribution-type BY.